

Undersampled Phase Retrieval with Outliers

Daniel S. Weller, *Member, IEEE*, Ayelet Pnueli, Gilad Divon, Ori Radzyner,
Yonina C. Eldar, *Fellow, IEEE*, and Jeffrey A. Fessler, *Fellow, IEEE*

Abstract—We propose a general framework for reconstructing transform-sparse images from undersampled (squared)-magnitude data corrupted with outliers. This framework is implemented using a multi-layered approach, combining multiple initializations (to address the nonconvexity of the phase retrieval problem), repeated minimization of a convex majorizer (surrogate for a nonconvex objective function), and iterative optimization using the alternating directions method of multipliers. Exploiting the generality of this framework, we investigate using a Laplace measurement noise model better adapted to outliers present in the data than the conventional Gaussian noise model. Using simulations, we explore the sensitivity of the method to both the regularization and penalty parameters. We include 1D Monte Carlo and 2D image reconstruction comparisons with alternative phase retrieval algorithms. The results suggest the proposed method, with the Laplace noise model, both increases the likelihood of correct support recovery and reduces the mean squared error from measurements containing outliers. We also describe exciting extensions made possible by the generality of the proposed framework, including regularization using analysis-form sparsity priors that are incompatible with many existing approaches.

EDICS Categories: CIF-SBR, CIF-SBI, CIF-OB1

I. INTRODUCTION

PHASE retrieval [1]–[3] refers to the problem of recovering a signal or image from magnitude-only measurements of a transform of that signal. This problem appears in crystallography [4]–[7], optical imaging [8], astronomical imaging [9], and other areas [10]–[14].

Phase retrieval is inherently ill-posed, as many signals may share the same magnitude spectrum [15]. To address this issue, existing phase retrieval algorithms incorporate different sources of prior information. The Gerchberg-Saxton error reduction method [16] of alternating projections uses magnitude information about both an image and its Fourier spectrum. Fienup’s hybrid input-output (HIO) algorithm [17], [18] generalizes the image domain projection of error reduction to other constraints such as image boundary and support information [19]–[21]. More recently, the alternating projections framework [22] has been extended to sparse reconstruction [23]–[25]; examples include compressive phase

DSW was funded by National Institutes of Health (NIH) grant F32 EB015914. JAF is funded in part by NIH grant P01 CA87634 and an equipment donation from Intel. YCE is funded in part by Israel Science Foundation Grant 170/10, SRC, and Intel Collaborative Research Institute for Computational Intelligence.

DSW is with the Charles L. Brown Department of Electrical and Computer Engineering, University of Virginia, Charlottesville, VA 22904 USA (email: dweller@virginia.edu). AP was with, and GD, OR, and YCE are with the Electrical Engineering Department, Technion, Israel Institute of Technology, Haifa 32000, Israel (emails: ayelet.pnueli@gmail.com, giladd44@gmail.com, radzy@campus.technion.ac.il, yonina@ee.technion.ac.il). JAF is with the Department of Electrical Engineering and Computer Science, University of Michigan, Ann Arbor, MI 48109 USA (email: fessler@umich.edu).

retrieval [26], [27] and the sparse Fienup method [28]. Other formulations forgo the HIO framework. One method uses rough phase estimates [29] to dramatically improve reconstruction quality. Another uses a matrix lifting scheme [30], [31] to construct a semidefinite relaxation of the phase retrieval problem [32], which may be combined with sparsity-promoting regularization [30], [33]–[36]. Other approaches employing sparsity for phase retrieval include the graph-based and convex optimization methods in [37] and greedy algorithms like GESPAR [38].

In addition to lacking phase information, measurements are often noisy, especially at the microscopic scales used in crystallography and optical imaging. Most existing methods either ignore measurement noise or impose quadratic data fit penalties. Our method, introduced first in [39], employs a 1-norm data fit term, corresponding to a Laplace noise model, designed to improve robustness to outliers. Our optimization framework combines a majorize-minimize algorithm with a nested variable-split and the alternating directions method of multipliers (ADMM) to solve the phase retrieval problem with a robust data fit model and 1-norm sparsity-promoting regularizer. Although the original problem is nonconvex, our proposed majorizer is convex and as tight as possible. While direct minimization of this majorizer would be combinatorially complex, introducing an auxiliary variable enables efficient minimization via ADMM. We compare our approach against using a conventional quadratic data fit term within our framework, separating the contributions of the implementation from the proposed noise model. We established earlier [39] that properly tuning the parameter for the 1-norm sparse regularization term is essential for successful reconstruction. Here, we thoroughly study the parameter selection problem, analyzing the regularization parameter as well as the ADMM penalty parameter that affects the convergence rate of the ADMM component of the algorithm.

Section II presents a general likelihood model for the phase retrieval problem. Section III introduces a convex majorizer for the optimization problem, and Sec. IV describes our solution to this convex subproblem using ADMM. After investigating the tuning of the regularization and penalty parameters in Sec. V, we present 1D Monte Carlo comparisons in Sec. VI, and a 2D image reconstruction in Sec. VII. We conclude with a discussion of the merits of our algorithm and future extensions. Code and data are available online from <http://people.virginia.edu/~dsw8c/sw.html>.

II. PROBLEM STATEMENT

Consider the standard phase retrieval problem, where a length- N (complex-valued) signal \mathbf{x} is reconstructed from M

squared-magnitude measurements $\mathbf{y} = [y_1, \dots, y_M]^T$ of the discrete Fourier transform (DFT) of \mathbf{x} :

$$y_m = |[\mathbf{A}\mathbf{x}]_m|^2 + \nu_m, \quad m = 1, \dots, M, \quad (1)$$

where $[\mathbf{A}\mathbf{x}]_m = \sum_{n=1}^N A_{mn}x_n$ is the m th DFT coefficient, and $[\nu_1, \dots, \nu_M]^T$ is a vector of additive white Gaussian noise. The vector \mathbf{x} may represent either a 1D signal or a higher dimensional image, columnized.

Our framework aims to minimize the negative log-likelihood function $\sum_{m=1}^M -\ell(y_m; |[\mathbf{A}\mathbf{x}]_m|^q)$. With Gaussian noise,

$$-\ell(y_m; |[\mathbf{A}\mathbf{x}]_m|^q) \propto |y_m - |[\mathbf{A}\mathbf{x}]_m|^q|^2. \quad (2)$$

This formulation generalizes standard phase retrieval in several ways. First, the linear transform \mathbf{A} can be any sensing matrix, not just the DFT. Second, the system may measure the magnitude or squared-magnitude of $[\mathbf{A}\mathbf{x}]_m$, or even more broadly, any power of the magnitude $|[\mathbf{A}\mathbf{x}]_m|^q$, for $q \geq 1$. Third, the measurement noise no longer is strictly Gaussian. To account for outliers in the data, we focus on using the Laplace distribution, with negative log-likelihood function

$$-\ell(y_m; |[\mathbf{A}\mathbf{x}]_m|^q) \propto |y_m - |[\mathbf{A}\mathbf{x}]_m|^q|. \quad (3)$$

Our method applies more broadly to log-likelihood functions of the form $-\ell([\mathbf{A}\mathbf{x}]_m; y_m) = f(h([\mathbf{A}\mathbf{x}]_m; y_m))$, where $f(\cdot)$ is convex and nondecreasing (on \mathbb{R}_+), and the data prediction error function $h(t; y) \triangleq |y - |t|^q|$, with $t \in \mathbb{C}$ and $y \in \mathbb{R}$. For this class of functions, the majorizer derived in Sec. III is convex in \mathbf{x} .

To resolve the ill-posedness of the phase retrieval problem, we impose a sparsity-promoting prior on the signal, using the 1-norm convex relaxation $\|\mathbf{x}\|_1$. Throughout this work, we focus on image sparsity, or equivalently, synthesis-form sparsity, by appending a synthesis transform to the sensing matrix \mathbf{A} . We seek the minimizer $\hat{\mathbf{x}} \in \mathbb{C}^N$ of the problem

$$\hat{\mathbf{x}} = \arg \min_{\mathbf{x} \in \mathbb{C}^N} \Psi(\mathbf{x}) \triangleq \sum_{m=1}^M f(h([\mathbf{A}\mathbf{x}]_m; y_m)) + \beta \|\mathbf{x}\|_1, \quad (4)$$

where $\beta > 0$ is the regularization penalty parameter. Our algorithm aims to find a sparse signal \mathbf{x} that is roughly consistent with the magnitude data.

Our formulation (4) differs from many of the methods described in the literature. First, the existing methods are not designed to accommodate the Laplace noise model, limiting their robustness to outliers. The projection-based methods, the semidefinite relaxations, and GESPAR all implicitly (via projections) or explicitly minimize the quadratic negative log-likelihood representing a Gaussian noise model. In addition, the GESPAR and sparse Fienup methods use 0-“norm” sparsity, while we use 1-norm sparsity-promoting regularization, also found in the convex relaxations recently developed.

III. MAJORIZATION OF THE MEASUREMENT OBJECTIVE

The inverse problem formulation of phase retrieval is particularly difficult to solve because having only magnitude information makes the data fit term in the objective function $\Psi(\mathbf{x})$ nonconvex. To facilitate optimization, we construct a convex majorizer for $\Phi(\mathbf{x})$. Section IV describes an iterative method for minimizing this majorizer effectively.

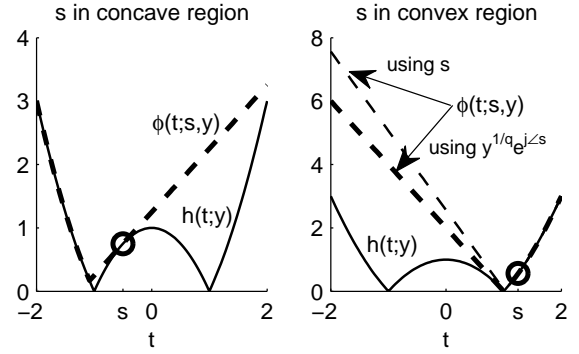


Fig. 1. The data fit error $h(t; y)$ (solid line) and the convex majorizer (surrogate) $\phi(t; s, y)$ (dashed line) are plotted for real t , $y = 1$, and $q = 2$. Circles highlight the majorization points s for both examples. In the left figure, the majorization point s is in the concave region of $h(t; y)$, so the tangent plane at s is used in this region. In the right figure, s is located in the convex region of $h(t; y)$, and the tangent plane at $y^{1/q}e^{i\angle s}$ is used instead.

A. Majorizing $\Psi(\mathbf{x})$

In general, a majorizer $\phi(t; s)$ for a function $h(t)$ satisfies two properties: $\phi(s; s) = h(s)$, and $\phi(t; s) \geq h(t)$, for all t . When these properties are satisfied, decreasing the value of the majorizer also decreases the value of the original function, since $h(t) \leq \phi(t; s) < \phi(s; s) = h(s)$.

Returning to our framework, assuming $f(\cdot)$ is convex and nondecreasing, and $\phi(\cdot)$ is a convex function, then $f(\phi(\cdot))$ is convex [40]. So, given a convex surrogate $\phi(t; s, y)$ for $h(t; y)$, $f(\phi(t; s, y))$ is convex. Furthermore, when $\phi(t; s, y)$ majorizes $h(t; y)$, $f(\phi(t; s, y))$ majorizes $f(h(t; y))$ as well. To find a convex majorizer $\phi(t; s, y)$, we first write $h(t; y)$ as

$$h(t; y) = \max\{h_+(t; y) \triangleq |t|^q - y, h_-(t; y) \triangleq y - |t|^q\}. \quad (5)$$

Assuming $q \geq 1$, $h_+(t; y)$ is already convex, but $h_-(t; y)$ is concave. When $y \leq 0$, $h(t; y) = h_+(t; y)$. But, whenever $y > 0$, $h_-(t; y)$ needs to be replaced with a convex majorizer $\phi_-(t; s, y)$. Then, $\phi(t; s, y) \triangleq \max\{h_+(t; y), \phi_-(t; s, y)\}$ is convex and majorizes $h(t; y)$.

Since $h_-(t; y)$ is concave, we employ as a convex surrogate its tangent plane about some point $s \in \mathbb{C}$:

$$\begin{aligned} \phi_-(t; s, y) &= (y - |s|^q) + (-q|s|^{q-1})\mathcal{R}\{e^{-i\angle s}(t - s)\} \\ &= y + (q - 1)|s|^q - q|s|^{q-1}\mathcal{R}\{te^{-i\angle s}\}. \end{aligned} \quad (6)$$

When $q = 1$, $h_-(t; y)$ is not differentiable at $t = 0$, but our definition in (6) is consistent with the tangent plane $\phi_-(t; s, y) = y$ in this context.

Since any other convex majorizer must lie above the tangent plane, (6) is clearly tight among possible convex majorizers of $h_-(t; y)$. However, when using $|s|^q > y$, we are in the convex region of $h(t; y)$, and we only need to majorize $h(t; y)$ in the concave region. In this case, the tangent plane $\bar{s} \triangleq y^{1/q}e^{i\angle s}$ still majorizes $h_-(t; y)$ in the range of $|t|^q \leq y$.

Our majorizer $\phi(t; s, y)$ is therefore given by

$$\phi(t; s, y) = \begin{cases} h_+(t; y), & y \leq 0, \\ \max\{h_+(t; y), \phi_-(t; s, y)\}, & 0 \leq |s|^q < y, \\ \max\{h_+(t; y), \phi_-(t; \bar{s}, y)\}, & 0 < y \leq |s|^q. \end{cases} \quad (7)$$

Algorithm 1 Majorize-minimize scheme for solving (4).

Require: I_{mm} , ϵ_{mm} , random $\mathbf{s}^0 \in \mathbb{C}^M$.
for $i = 1 : I_{\text{mm}}$ **do**
 $\mathbf{x}^i \leftarrow \arg \min_{\mathbf{x}} \Phi(\mathbf{x}; \mathbf{s}^{i-1})$. (9)
 $\mathbf{s}^i \leftarrow \mathbf{A}\mathbf{x}^i$. (10)
if $\|\mathbf{s}^i - \mathbf{s}^{i-1}\| < \epsilon_{\text{mm}}$ **then break**
end if
end for

The first case occurs when $h(t; y)$ is already convex ($|t|^q$ cannot be less than y). The second and third cases correspond to s being in the concave and convex regions of $h(t; y)$, respectively. Figure 1 portrays examples of the function $h(t; y)$ and its surrogate $\phi(t; s, y)$ in both the second (s in concave region) and third (s in convex region) cases. Substituting $\phi(t; s, y)$ for $h(t; y)$ in the original objective yields our complete convex surrogate $\Phi(\mathbf{x}; \mathbf{s})$ for $\Psi(\mathbf{x})$:

$$\Phi(\mathbf{x}; \mathbf{s}) = \sum_{m=1}^M f(\phi([\mathbf{A}\mathbf{x}]_m; s_m, y_m)) + \beta \|\mathbf{x}\|_1. \quad (8)$$

B. Majorize-Minimize Algorithm

Our proposed majorized approach to minimizing $\Psi(\mathbf{x})$ in (4) repeatedly minimizes $\Phi(\mathbf{x}; \mathbf{s})$, using the majorize-minimize [41], [42] scheme shown in Algorithm 1. Although each iteration of this majorize-minimize method decreases $\Psi(\mathbf{x})$, convergence to a minimum of $\Psi(\mathbf{x})$ is not guaranteed, since the majorizer may get “stuck” at a critical point of $\Psi(\mathbf{x})$, like the local maximum at $t = 0$. Since the original problem is nonconvex, running the algorithm for multiple different initializations increases the chance of finding a global optimum while decreasing the likelihood of failure due to stagnation. Employing multiple initializations is frequently employed by other phase retrieval methods and when solving nonconvex problems more generally.

IV. SOLVING THE MAJORIZED OBJECTIVE WITH ADMM

Jointly minimizing M pairwise maximum functions to solve (8) directly would be combinatorially complex. Instead, we introduce an auxiliary vector $\mathbf{u} = \mathbf{A}\mathbf{x}$ to un-mix $\mathbf{A}\mathbf{x}$ and ensure each function in the summation in (8) depends only on a single $u_m = [\mathbf{u}]_m$. The constrained optimization problem using this auxiliary variable is

$$\begin{aligned} \{\mathbf{x}^{i+1}, \mathbf{u}\} \leftarrow \arg \min_{\mathbf{x}, \mathbf{u}} \sum_{m=1}^M f(\phi(u_m; s_m, y_m)) + \beta \|\mathbf{x}\|_1, \\ \text{s.t. } u_m = [\mathbf{A}\mathbf{x}]_m, \quad m = 1, \dots, M. \end{aligned} \quad (11)$$

We use the alternating directions method of multipliers (ADMM) [43]–[46] framework to solve the augmented Lagrangian form of this constrained problem:

$$\begin{aligned} \mathcal{L}_A(\mathbf{x}, \mathbf{u}; \mathbf{b}) \triangleq \sum_{m=1}^M f(\phi(u_m; s_m, y_m)) + \beta \|\mathbf{x}\|_1 \\ + \frac{\mu}{2} \|\mathbf{A}\mathbf{x} - \mathbf{u} + \mathbf{b}\|_2^2, \end{aligned} \quad (12)$$

Algorithm 2 ADMM method for solving (12).

Require: I_{ADMM} , ϵ_{ADMM} , \mathbf{x}^0 , \mathbf{u}^0 , \mathbf{y} , β , μ .
 $\mathbf{b}^0 \leftarrow \mathbf{A}\mathbf{x}^0 - \mathbf{u}^0$.
for $i = 1 : I_{\text{ADMM}}$ **do**
 $\mathbf{x}^i \leftarrow \arg \min_{\mathbf{x}} \beta \|\mathbf{x}\|_1 + \frac{\mu}{2} \|\mathbf{A}\mathbf{x} - (\mathbf{u}^{i-1} - \mathbf{b}^{i-1})\|_2^2$. (13)
 for $m = 1 : M$ **do**
 $d_m \leftarrow [\mathbf{A}\mathbf{x}^i + \mathbf{b}^{i-1}]_m$.
 $u_m^i \leftarrow \arg \min_u f(\phi(u; s_m, y_m)) + \frac{\mu}{2} |u - d_m|^2$. (14)
 end for
 $\mathbf{b}^i \leftarrow \mathbf{b}^{i-1} + (\mathbf{A}\mathbf{x}^i - \mathbf{u}^i)$. (15)
 if $\|\mathbf{x}^i - \mathbf{x}^{i-1}\| < \epsilon_{\text{ADMM}}$ **then break**
 end if
end for

Algorithm 3 FISTA implementation for solving (13).

Require: I_{FISTA} , \mathbf{x}^0 , \mathbf{u} , \mathbf{b} , β , μ .
 $\mathbf{z}^0 \leftarrow \mathbf{x}^0$, $t^0 \leftarrow 1$, and compute c such that $c\mathbf{I} \succeq \mu\mathbf{A}'\mathbf{A}$.
for $i = 1 : I_{\text{FISTA}}$ **do**
 $\mathbf{x}^i \leftarrow \text{soft}(\mathbf{z}^{i-1} + \frac{\mu}{c}\mathbf{A}'(\mathbf{u} - \mathbf{b} - \mathbf{A}\mathbf{z}^{i-1}); \frac{\beta}{c})$. (17)
 $t^i \leftarrow (1 + \sqrt{1 + 4(t^{i-1})^2})/2$. (18)
 $\mathbf{z}^i \leftarrow \mathbf{x}^i + \frac{t^{i-1}-1}{t^i}(\mathbf{x}^i - \mathbf{x}^{i-1})$. (19)
end for

where $\mathbf{b} \in \mathbb{C}^M$ and $\mu > 0$ are the scaled dual vector (Lagrange multipliers) and augmented Lagrangian penalty parameter, respectively. Our implementation of ADMM in Algorithm 2 solves (12). We define $d_m = [\mathbf{A}\mathbf{x} + \mathbf{b}]_m$ to simplify notation here and in subsequent sections. We initialize ADMM using the last \mathbf{x} from the previous iteration of the majorize-minimize algorithm. Then, $\mathbf{u}^0 \leftarrow \mathbf{A}\mathbf{x}^0$, leaving $\mathbf{b}^0 = \mathbf{0}$. Methods for updating \mathbf{x} and \mathbf{u} depend on the specific \mathbf{A} and $f(\cdot)$ used. We provide details for the range of cases explored in this paper.

A. Updating \mathbf{x}

The update for \mathbf{x} in the preceding ADMM framework has the standard synthesis form of compressed sensing (CS) that has been extensively studied previously [47]–[49]. Various CS algorithms may be appropriate, depending on \mathbf{A} 's structure.

If \mathbf{A} is left-unitary, so $\mathbf{A}'\mathbf{A} = \mathbf{I}$, the least-squares term in (13) simplifies to $\|\mathbf{x} - \mathbf{A}'(\mathbf{u}^i - \mathbf{b}^i)\|_2^2$, plus a constant term (zero when \mathbf{A} is also right-unitary), and updating \mathbf{x} becomes soft thresholding: $\mathbf{x}_n^{i+1} \leftarrow \text{soft}([\mathbf{A}'(\mathbf{u}^i - \mathbf{b}^i)]_n; \frac{\beta}{\mu})$, where

$$\text{soft}(x; \tau) = \frac{x}{|x|} \max\{|x| - \tau, 0\}. \quad (16)$$

When \mathbf{A} is not left-unitary, an iterative algorithm like FISTA [50] may be nested within the ADMM method. Algorithm 3 describes the FISTA implementation that approximately solves (13). When \mathbf{A} is left or right unitary, $c = \mu$. In other cases, c is the maximum singular value of \mathbf{A} and may be precomputed using power iterations.

This framework can be extended to analysis-form sparsity and other additively separable regularizers by replacing the penalty $\|\mathbf{x}\|_1$ in the original objective (4), the majorizer (8), and the augmented Lagrangian (12) with the prior $R(\mathbf{G}\mathbf{x}) = \sum_i r([\mathbf{G}\mathbf{x}]_i)$, where $r(\cdot)$ is a potential function, and \mathbf{G} is an analysis transform. The \mathbf{x} -update step for ADMM becomes

$$\mathbf{x}^{i+1} \leftarrow \arg \min_{\mathbf{x}} \beta R(\mathbf{G}\mathbf{x}) + \frac{\mu}{2} \|\mathbf{A}\mathbf{x} - (\mathbf{u}^i - \mathbf{b}^i)\|_2^2. \quad (20)$$

When \mathbf{G} is square and invertible, and the inverse \mathbf{G}^{-1} is readily available, synthesis-form techniques apply. Otherwise, one may nest within the ADMM framework almost any of the well-studied methods from the literature such as split Bregman iteration [51] or analysis-form extensions of iterative methods like MFISTA [52]–[54]. When the proximal operator for $r(\cdot)$ does not have a closed form, proximal algorithms may also be used [55]. Alternatively, one may “smooth” a nonsmooth regularizer (using corner rounding), and apply gradient-based methods like nonlinear conjugate gradients [56].

In any case, we can leverage the substantial literature on sparse reconstruction to update \mathbf{x} within our ADMM framework. By using a majorizer and variable-splitting, we cast the sparse regularization component of the reconstruction problem in this well-studied form, without regard to the noise model used in the data fit term of the original problem.

B. Updating u

An important consequence of the choice of variable-splitting is that the objective function for updating the auxiliary vector \mathbf{u} is additively separable. Thus, the update can be performed element-by-element. Since $f(\cdot)$ is monotone non-decreasing, and $\phi(u; s_m, y_m)$ is the pointwise maximum of two functions (for $y > 0$), we can write $f(\phi(u; s_m, y_m))$ as $\max\{f_+(u), f_-(u)\}$, where

$$f_+(u) \triangleq \frac{\mu}{2} |u - d_m|^2 + f(h_+(u; y_m)), \quad (21)$$

$$f_-(u) \triangleq \frac{\mu}{2} |u - d_m|^2 + \begin{cases} 0, & y \leq 0, \\ f(\phi_-(u; s_m, y_m)), & 0 \leq |s|^q < y, \\ f(\phi_-(u; \bar{s}_m, y_m)), & 0 < y \leq |s|^q, \end{cases} \quad (22)$$

and $d_m = [\mathbf{A}\mathbf{x} + \mathbf{b}]_m$. Updating u_m is equivalent to solving

$$\arg \min_{u, T} T, \text{ s.t. } f_+(u) \leq T, f_-(u) \leq T. \quad (23)$$

The minimizing T corresponds to the function value of $f(\phi(u; s_m, y_m))$ at its minimum. The Lagrangian of this constrained problem is $T + \gamma_+(f_+(u) - T) + \gamma_-(f_-(u) - T)$, with Lagrange multipliers $\gamma_+, \gamma_- \geq 0$. Differentiating yields $\gamma_+ + \gamma_- = 1$, and three possibilities exist:

- 1) When $\gamma_+ = 1$, and $\gamma_- = 0$, $f_+(u) = T$, and $f_-(u) < T$, so the optimal $u = u_+$ minimizes $f_+(u)$ and satisfies $f_+(u_+) > f_-(u_+)$.
- 2) When $\gamma_+ = 0$, and $\gamma_- = 1$, the optimal $u = u_-$ minimizes $f_-(u)$ and satisfies $f_-(u_-) > f_+(u_-)$.
- 3) When $\gamma_+, \gamma_- > 0$, both $f_+(u)$ and $f_-(u)$ equal T . The optimal $u = u_{\pm}$ minimizes both of these functions along the curve $f_+(u) = f_-(u)$.

The optimal values of u for each case are computed analytically for $f(\cdot)$ corresponding to the Gaussian and Laplace distribution functions in (2) and (3) on squared-magnitude measurements ($q = 2$). Dropping subscripts, for $p = 1, q = 2$,

$$u_+ = \frac{\mu}{2+\mu} d, \quad (24)$$

$$u_- = \frac{2s}{\mu} + d, \text{ and} \quad (25)$$

$$u_{\pm} = \sqrt{2(y + |s|^2)} e^{i\angle((2+\mu)s + \mu d)} - s. \quad (26)$$

For $p = q = 2$,

$$u_+ = \text{root}([4, 0, (\mu - 4y), -\mu|d|]) e^{i\angle d}, \quad (27)$$

$$u_- = (\mathcal{R}e\{\bar{u}\} + i\mathcal{I}m\{\bar{u}\}) e^{i\angle s}, \quad (28)$$

$$u_{\pm} = (c_0 e^{i\theta} - \bar{s}) e^{i\angle s}, \text{ where } c_0 = \sqrt{2(y + |s|^2)}, \quad (29)$$

$$\theta = \text{root}([(r_2/r_1 \sin \alpha), (2r_2/r_1 \cos \alpha + 4), 0,$$

$$(2r_2/r_1 \cos \alpha - 4), -r_2/r_1 \sin \alpha]),$$

$$c_1 = c_0^2 + |s|^2 - y, r_1 = 2c_0|s|,$$

and r_2 and α are the magnitude and phase of

$$c_0(4c_1|s| + \mu(|s| + d e^{-i\angle s})).$$

When calculating u_+ and u_{\pm} for the Gaussian case, the root used is the one whose corresponding u minimizes $f_+(u)$. These expressions are derived in the appendices.

V. PARAMETER TUNING

The regularization parameter β controls the level of sparsity in the reconstructed signal. Additionally, the ADMM penalty parameter μ impacts the convergence rate of the inner ADMM algorithm, and thus, the overall algorithm. This section explores the influence of these parameters.

Our simulations consist of generating a length- N sparse signal with K nonzero coefficients, M measurements of the DFT of that signal, performing the reconstructions, and comparing the reconstructed signals against the true signal. The sparse support of our signal is chosen at random, and the amplitude and phase of each of nonzero coefficient are randomly sampled uniformly between 0.5 and 1 (for amplitude) and 0 and 2π (for phase). Then, M noise-free measurements are randomly selected from the squared-magnitude of the signal’s DFT coefficients. Randomly selected outliers are set to have an amplitude of twice the maximum measurement. This model does not exactly match our Laplace noise model, thus avoiding an “inverse crime.” The reconstructions are performed using multiple initializations, and the “best” reconstructed signal for each method is retained. For the proposed method, the best reconstruction yields the lowest value of $\Psi(\mathbf{x})$.

Sparsity and Fourier coefficient magnitudes are insensitive to spatial shifts, reversal, and global phase, so we find the best alignment/reversal and global phase for the reconstructed signals before evaluation. The best alignment is identified for both the reconstructed signal and its reversed version by cross-correlation with the true signal. A global phase term is then estimated from the version with the best alignment. For evaluation, a sparse threshold of 0.05 is used to identify the sparse support of the reconstructed signal. The sparse support of a correctly detected signal matches that of the true signal.

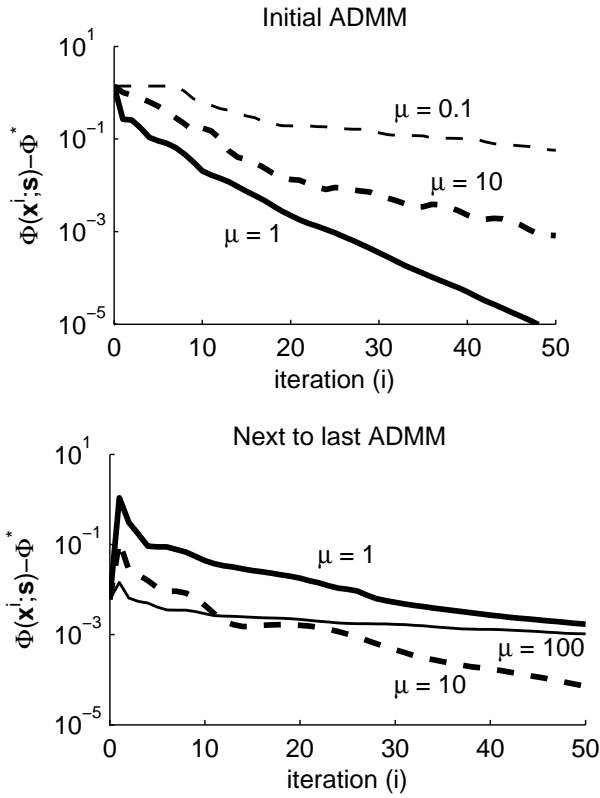


Fig. 2. The objective function $\Phi(x^i; s)$, relative to converged objective value Φ^* , is plotted versus ADMM iteration i for both the first and the next-to-last run of ADMM, for the Laplace ($p = 1$) noise model.

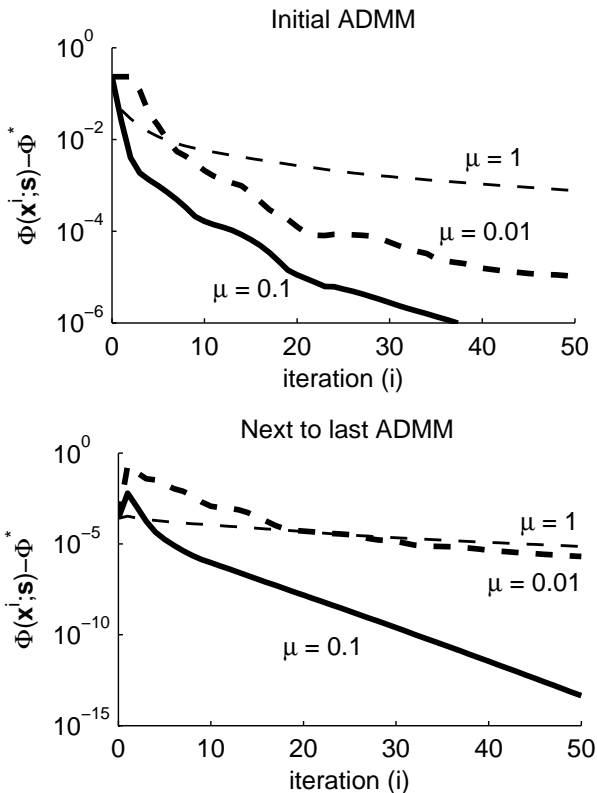
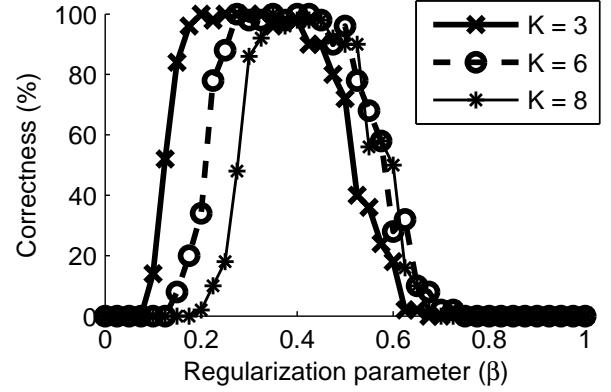
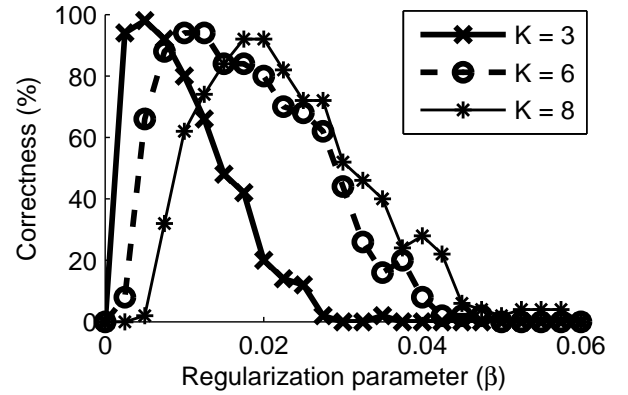


Fig. 3. The objective function $\Phi(x^i; s)$, relative to converged objective value Φ^* , is plotted versus ADMM iteration i for both the first and the next-to-last run of ADMM, for the Gaussian ($p = 2$) noise model.



(a) Laplace ($p = 1$) noise model.



(b) Gaussian ($p = 2$) noise model.

Fig. 4. The percentage of 50 trials reconstructed correctly is plotted versus regularization parameter β for varying signal sparsity levels K , for the proposed reconstruction with (a) Laplace ($p = 1$) and (b) Gaussian ($p = 2$) noise models.

In our first experiment, we reconstruct a 128-element 1D signal using both Laplace ($p = 1$) and Gaussian noise models ($p = 2$) and ADMM with different values of penalty parameter μ , for different degrees of sparsity and numbers of measurements. Since the optimal ADMM parameter may differ between earlier and later majorizer minimization iterations, we compare the convergence rates for different choices of μ in both the initial and next-to-last runs of ADMM. Figures 2 and 3 portray, for sparsity $K = 6$, $M = 64$ noiseless measurements, and Laplace ($p = 1$) and Gaussian ($p = 2$) noise models, respectively, the objective function convergence rates over $I_{\text{ADMM}} = 50$ ADMM iterations for the three best choices of μ , relative to the best objective function value observed over 200 ADMM iterations. Running the same experiment for different sparsity $K = 8$ and $M = 128$ measurements yield similar results to the example shown, with the same optimal μ 's. In this experiment, we observe the optimal choice of μ for the proposed method with $p = 1$ does not change much from the initial to the next-to-last run of ADMM, changing only from $\mu = 1$ to $\mu = 10$. However, a minor change in μ can make a huge difference in convergence rate, especially in later iterations, so using an adaptive scheme like the heuristic method described in [46] would help maintain fast convergence. The optimal choice of μ appears more stable in

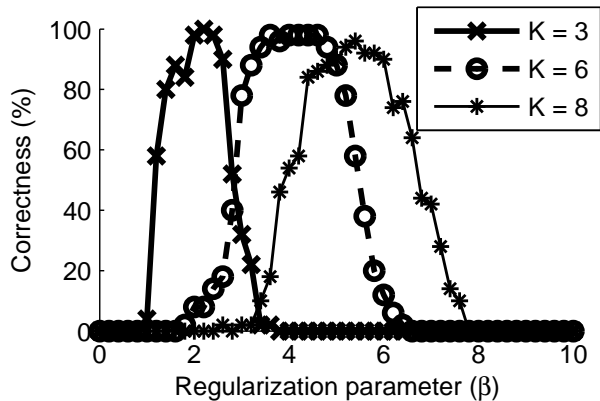


Fig. 5. The percentage of 50 trials reconstructed correctly is plotted for the modified sparse Fienup (L_1 -Fienup) method that projects the image domain reconstruction onto the 1-norm ball $\|\mathbf{x}\|_1 \leq \beta$, versus constraint parameter β for varying signal sparsity levels K .

the $p = 2$ case, as $\mu = 0.1$ yields the fastest objective function convergence for both early and later runs. The optimal choices of μ in both instances do not appear to change with sparsity K or number of measurements M , or the associated changes in β , so we used these values of μ throughout the experiments that follow.

To study the effects of varying β on the performance of the algorithm, we focus on reconstructing 1D signals using either Laplace or Gaussian noise models for varying degrees of sparsity. Here, we used 40 random initializations for both $p = 1$ and $p = 2$ cases. In [39], the optimal range of β for the proposed method with $p = 1$, $q = 2$ is shown to scale roughly linearly with the number of measurements. Here, we evaluate the proposed method with both Laplace and Gaussian noise models for $M = N = 128$ noise-free measurements. Figure 4 plots the percentage of 50 trials reconstructed with the correct support versus the regularization parameter for different sparsity levels $K = 3, 6, 8$, for both noise models.

For comparison, we also evaluate the sparse Fienup method, with the image-domain projection modified to project the signal onto the 1-norm ball with $\|\mathbf{x}\|_1 \leq \beta$, for different values of regularization parameter β in Fig. 5. This modification replaces the hard-thresholding sparse projection onto the 0-“norm” ball with a 1-norm projection more closely aligned with the sparsity penalty used in the proposed method. We call this modified method L_1 -Fienup in the results that follow.

This L_1 -Fienup method exemplifies the great importance the choice of β has on the reconstruction quality. Not only does β greatly influence the chance of correct support detection, but the optimal choice of β greatly depends on the sparsity K of the signal. The optimal β for $K = 8$ would work extremely poorly for $K = 3$, and vice versa. The dependence on β of the proposed method is very similar, for both noise models. The $p = 1$ case demonstrates less variation in the correctness as a function of β than the $p = 2$ case, but a reasonably good choice of β is necessary for correct reconstruction with either noise model. The optimal choices of β were computed for all the values of K , without noise, used in the experiments that follow, including the 2D image comparisons.

TABLE I
COMPARISON OF RECONSTRUCTION METHODS

Method	Implementation	Sparsity	Noise Model
L_1 -Fienup	alternating projections	1-norm	Gaussian
Proposed ($p = 2$)	MM, ADMM	1-norm	Gaussian
GESPAR	greedy	0-“norm”	Gaussian
Proposed ($p = 1$)	MM, ADMM	1-norm	Laplace

VI. MONTE CARLO COMPARISONS (1D)

We compared phase retrieval methods using Monte Carlo simulations for different values of sparsity K and number of measurements M , with 50 trials each. We compare the proposed method with both $p = 1$ (Laplace) and $p = 2$ (Gaussian) data fit models against both the L_1 -Fienup method described previously and the GESPAR greedy method recently developed for the Gaussian noise model. Table I highlights the differences between the four methods.

These methods all use multiple initializations, with 40 initializations for L_1 -Fienup and the proposed method with $p = 1$, and with 50 initializations for the proposed method with $p = 2$. The GESPAR method tests different initializations until the sparse signal achieves data discrepancy below a fixed threshold. The percentage of trials with correctly reconstructed (detected) signal supports is shown for all four methods in Fig. 6, as a function of both number of measurements M (with five outliers) and sparsity of the true signal K . In addition, the average mean squared error (MSE) is reported in Fig. 7 in terms of peak signal to noise ratio, $\text{PSNR} = 10 \log_{10} \frac{1}{\text{MSE}}$, where the maximum true signal amplitude is one. To achieve the results shown, we had to increase the support detection threshold to 0.2 for the proposed method with $p = 2$ only, suggesting inadequate convergence for the Gaussian model.

These results suggest that the proposed method with the Laplace model $p = 1$, which more closely models the outliers in the measurements, attains the best performance of the four methods tested, in terms of both support recovery and PSNR. Figure 8 depicts trends in the correctness and PSNRs of the four methods as the number of outliers increases.

VII. IMAGE COMPARISONS (2D)

To demonstrate how the proposed method performs for image reconstruction, we examine the two-dimensional case with undersampled measurements corrupted by 10 outliers. The 512×512 -pixel star of David phantom used in [39] is inspired by the real example image shown in [57]. The DFT of this image is randomly undersampled by a factor of two and reconstructed using both the proposed and the state-of-the-art algorithms. The reconstruction using the proposed method with the Laplace model produces a nearly-perfect image. The L_1 -Fienup method yields an image with degraded or missing dots, especially in the lower left and right triangles, and near the top. The proposed method with a Gaussian model produces a more consistent reconstruction than the L_1 -Fienup method, but a number of additional dots near the center are visible. The $p = 2$ case shown uses $\mu = 1$; setting $\mu = 0.1$ degrades reconstruction quality in this case.

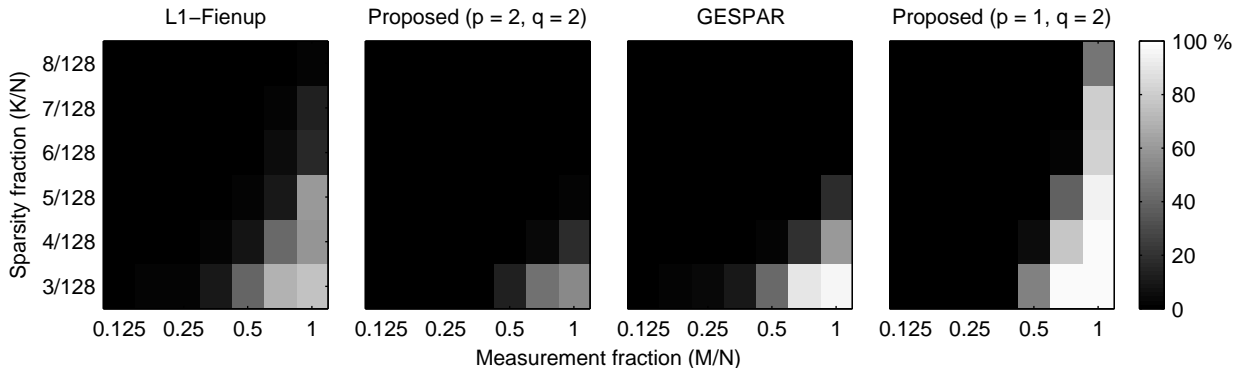


Fig. 6. The percentage of 50 trials reconstructed correctly is given for the modified sparse Fienup (L_1 -Fienup) method, GESPAR, and the proposed method with both Gaussian $p = 2$ and Laplace $p = 1$ noise models, for a range of measurement and sparsity fractions.

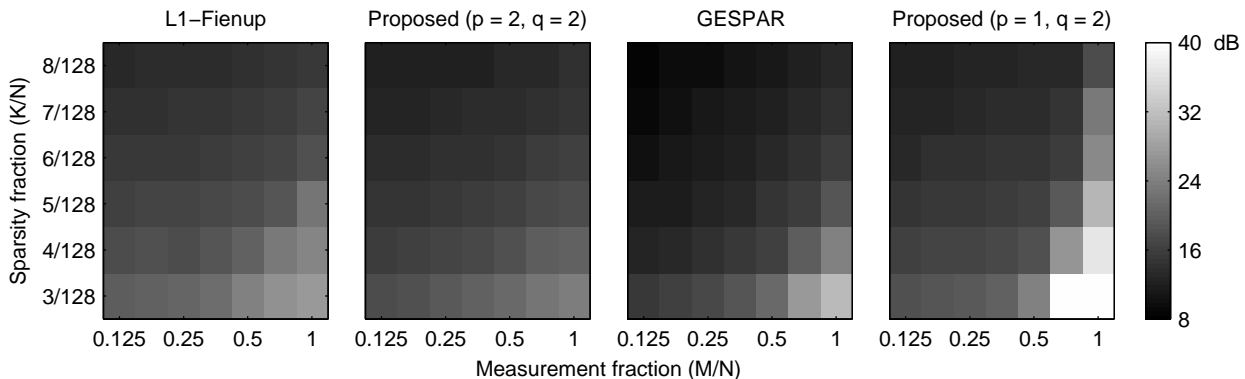


Fig. 7. The average PSNR, in dB, over 50 trials is given for the modified sparse Fienup (L_1 -Fienup) method, GESPAR, and the proposed method with both Gaussian $p = 2$ and Laplace $p = 1$ noise models, for a range of measurement and sparsity fractions.

VIII. DISCUSSION

Phase retrieval relies heavily on side information to reproduce a quality image. We employ sparsity in the image domain, or dictionary-based sparsity, to identify the best image among all those that share the same magnitude Fourier spectrum. Resolving this ambiguity becomes even more challenging in the face of measurement noise, especially outliers, and undersampling the Fourier spectrum. The proposed method using a Laplace noise model excels at reconstructing images despite these conditions, greatly improving upon other techniques and the Gaussian noise model for such data.

Parameter tuning does not appear to be more challenging than with existing methods in our simulations, especially considering the actual sparsity K usually is not known. Future research concerning automatic calibration and generalization of parameter selection is ongoing [58], and phase retrieval would appear to be an excellent application, based on its sensitivity to the choice of regularization parameter β . Additionally, using an adaptive heuristic for the penalty parameter μ appears to offer satisfactory convergence without substantial additional tuning. Further experiments on larger sets of different data are necessary, however, to draw more general conclusions about these parameters.

Paired with parameter selection, multiple initializations are also essential to overcome the nonconvexity of the inverse problem and find a reasonable (hopefully) global solution.

Although we investigated promising techniques for initializing our method, like Wirtinger flow [59], randomly selecting multiple initial majorization vectors s^0 appears to be more robust. However, using multiple initial choices for s^0 proportionally increases in computational burden. Combined with the multi-layered nature of the proposed algorithm, the overall reconstruction time becomes an issue in higher dimensions. In the 2D image reconstruction case, running a reconstruction for a single choice of β (and multiple choices were used for parameter tuning reasons) consumed several hours on a modern processor running MATLAB. Efforts to accelerate convergence of the proposed algorithm, such as applying momentum [60], would be well worth further study.

Computational costs aside, our method clearly outperforms the L_1 -modified Fienup method and GESPAR, when outliers are present in the data. Our method improves both the likelihood of correct support recovery and the overall normalized MSE in both 1D Monte Carlo and 2D image simulations.

Our framework may extend to more general regularizers $R(Gx)$ via generalization of the x -update step to nest an algorithm like split Bregman iteration. Such a modification would enable analysis-form sparsity regularization with total variation or undecimated wavelets. The x -update step also can accommodate other priors or constraints, like support information or nonnegativity, by using an appropriate nested algorithm in place of soft-thresholding or FISTA.

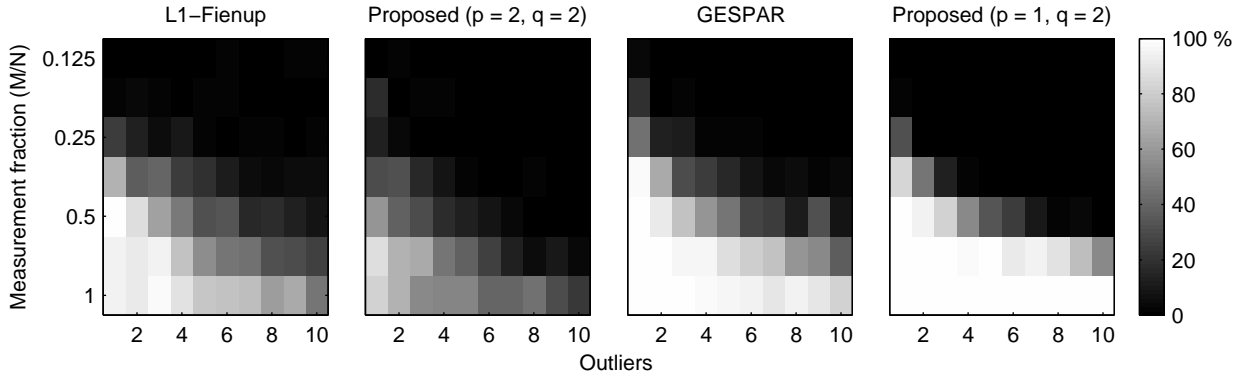
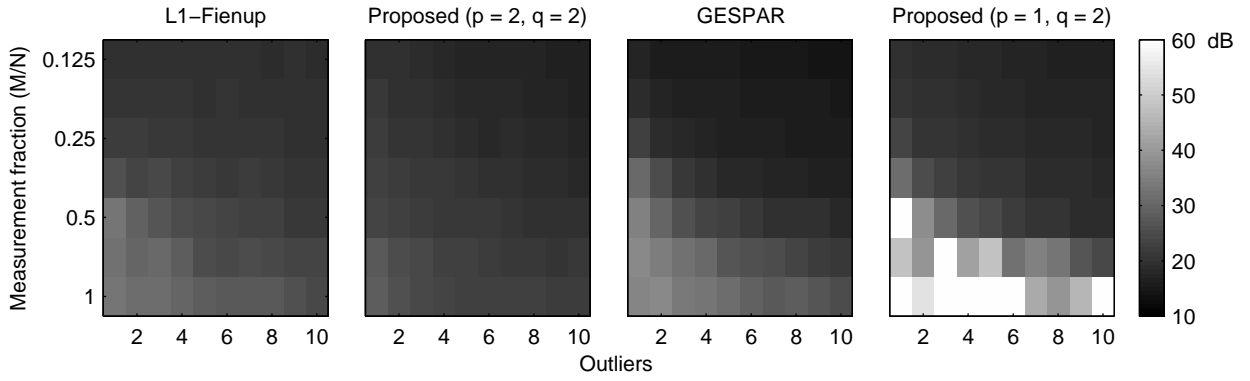
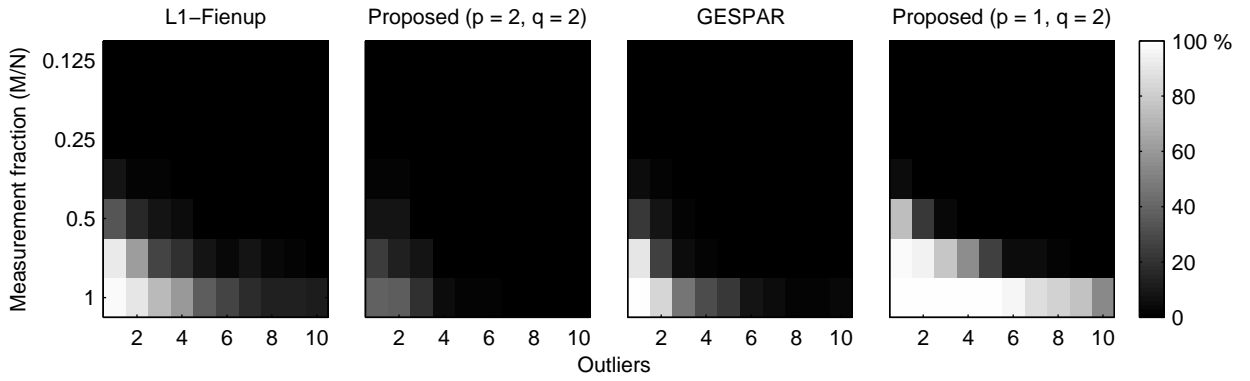
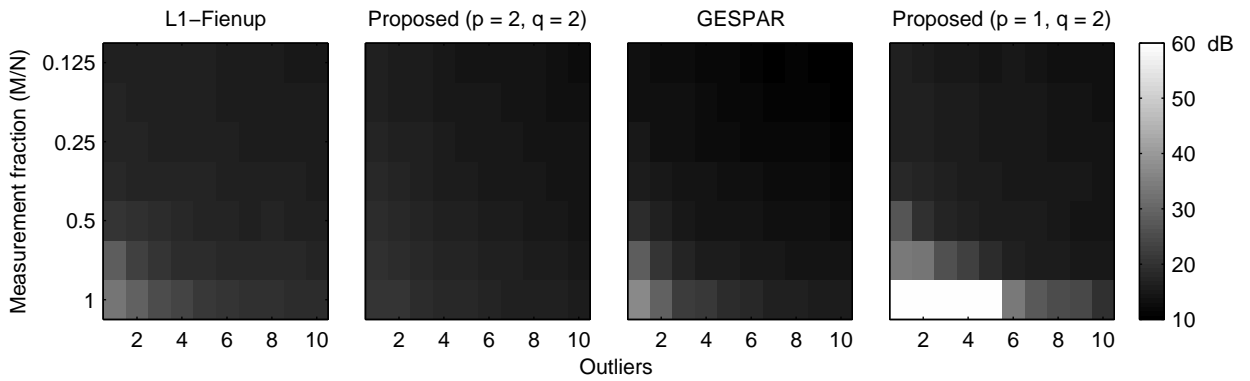
(a) Percentage of correct detections for $K = 3$ sparsity (out of $N = 128$)(b) PSNRs (in dB) for $K = 3$ sparsity (out of $N = 128$)(c) Percentage of correct detections for $K = 5$ sparsity (out of $N = 128$)(d) PSNRs (in dB) for $K = 5$ sparsity (out of $N = 128$)

Fig. 8. The correctness and average PSNR, in dB, are plotted for 50 trials of the L_1 -Fienup, GESPAR, and proposed algorithm with both models, for between 1 and 10 outliers out of $M = 16$ to $M = 128$ measurements, for $N = 128$ -length signals with sparsities $K = 3$ (top) and $K = 5$ (bottom).

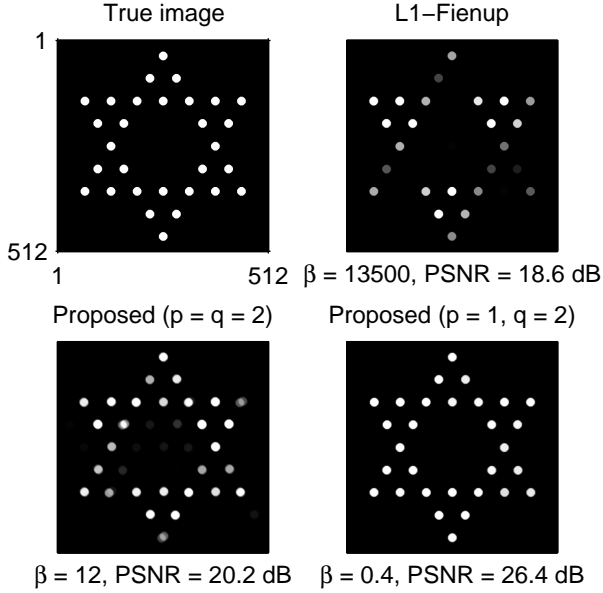


Fig. 9. The best reconstructions (as a function of regularization parameter β) for L1-Fienup and the proposed method with both noise models are shown for the 512×512 -pixel star of David phantom, from $M = N/2$ measurements, with 10 outliers.

IX. CONCLUSION

The key contributions of this paper are two-fold. First, a general framework was proposed that extends phase retrieval reconstruction to measurements corrupted by outliers in the data. A multi-layered implementation of this general framework was developed featuring multiple initializations, majorization-minimization, and ADMM. Secondly, the sensitivities to both the regularization and penalty parameters present in the reconstruction framework and algorithms were studied, aiming to provide a fast, robust, and correct reconstruction method. The analysis of the proposed method then shifted to a direct comparison against competing methods including an L1-modified sparse Fienup method and the greedy algorithm known as GESPAR. These comparisons included both a 1D Monte Carlo experiment to establish quantitative advantages over existing methods, and a 2D image reconstruction visually demonstrating the improvements achievable using this method, even with relatively few outliers in the data.

APPENDIX A

UPDATING u : SQUARED-MAGNITUDE LAPLACE CASE

In this case, $f(\cdot) = (\cdot)$, and $q = 2$. When $y_m < 0$, $f_+(u)$ is always greater than $f_-(u)$, so the solution is always the minimizer of $f_+(u)$. Otherwise, we must consider all three cases.

Let $d = [\mathbf{A}\mathbf{x}^{i+1} + \mathbf{b}^i]_m$, s represent the appropriate choice of s_m or \bar{s}_m , $\eta \triangleq \mu/2$, and drop the subscripts. Writing out $f_+(u)$ and $f_-(u)$,

$$\begin{aligned} f_+(u) &= \eta|u - d|^2 + |u|^2 - y, \\ f_-(u) &= \eta|u - d|^2 + y + |s|^2 - 2|s|\mathcal{R}e\{ue^{-i\angle s}\}. \end{aligned}$$

The function $f_+(u)$ is quadratic in u , so completing the square yields

$$f_+(u) = (1 + \eta)|u - \frac{\eta}{1+\eta}d|^2 + (\frac{\eta}{1+\eta}|d|^2 - y).$$

Thus, $f_+(u)$ is minimized by $u_+ = \frac{\eta}{1+\eta}d$.

The function $f_-(u)$ is also a quadratic, so

$$f_-(u) = \eta|u - e|^2 + (y + |s|^2 + \eta|d|^2 - \eta|e|^2),$$

where $e \triangleq \frac{s}{\eta} + d$. The minimizer is simply $u_- = e$.

The minimization of $f_+(u)$ or $f_-(u)$ along the curve on which both functions are equal-valued, involves parameterizing this curve and minimizing $f_+(u)$ as a function of this parameter. These functions are equal when $|u|^2 - y = y + |s|^2 - 2|s|\mathcal{R}e\{ue^{-i\angle s}\}$, which corresponds to the circle $|u + s|^2 = 2(y + |s|^2)$. The parameterization then corresponds to the angle along the circle; call it θ . The curve of interest is $(u+s) = \sqrt{2(y + |s|^2)}e^{i\theta}$. Incorporating this parameterization into $f_+(u)$ yields

$$\begin{aligned} f_+(u(\theta)) &= -2\sqrt{2(y + |s|^2)}\mathcal{R}e\{((1 + \eta)s + \eta d)e^{-i\theta}\} \\ &\quad + \text{constants}, \end{aligned}$$

which is minimized when $\theta = \angle((1 + \eta)s + \eta d)$. So, $u_{\pm} = \sqrt{2(y + |s|^2)}e^{i\angle((1+\eta)s+\eta d)} - s$.

APPENDIX B

UPDATING u : SQUARED-MAGNITUDE GAUSSIAN CASE

In this case, $f(\cdot) = (\cdot)^2$, and $q = 2$. Again, as with the Laplace distribution, when $y_m < 0$, $f_+(u) > f_-(u)$, so we always minimize $f_+(u)$. Otherwise, we consider all three cases.

Again, let $d = [\mathbf{A}\mathbf{x}^{i+1} + \mathbf{b}^i]_m$, s represent the appropriate choice of s_m or \bar{s}_m , $\eta \triangleq \mu/2$, and drop the subscripts. Writing out $f_+(u)$ and $f_-(u)$,

$$\begin{aligned} f_+(u) &= \eta|u - d|^2 + (|u|^2 - y)^2, \\ f_-(u) &= \eta|u - d|^2 + (y + |s|^2 - 2|s|\mathcal{R}e\{ue^{-i\angle s}\})^2. \end{aligned}$$

Writing $f_+(u)$ in terms of the magnitude $|u|$ and phase $\angle u$ of u ,

$$\begin{aligned} f_+(u) &= \eta|u|^2 + \eta|d|^2 - 2\eta|u||d|\cos(\angle u - \angle d) \\ &\quad + |u|^4 - 2y|u|^2 + y^2, \end{aligned}$$

which is clearly minimized when $\angle u = \angle d$, when $\cos(\angle u - \angle d) = 1$. Then, $f_+(u)$ becomes a quartic equation in $|u|$, which has the derivative

$$\frac{df_+(u)}{d|u|} = 4|u|^3 + (2\eta - 4y)|u| - 2\eta|d|.$$

The function $f_+(u)$ is minimized either when the derivative is zero or when $|u| = 0$. The depressed cubic equation will have between zero and three nonnegative real roots, which can be found analytically. Note that if there are three positive real roots, since the cubic must be increasing below the least positive root, the derivative at $|u| = 0$ is negative, and the fourth candidate point $|u| = 0$ cannot be the global minimum. The minimizer u_+ is the candidate point with minimum function value $f_+(|u|)$, multiplied by $e^{i\angle d}$.

Finding a minimum of $f_-(u)$ is straightforward. Define $\bar{u} = ue^{-i\angle s}$, and $\bar{d} = de^{-i\angle s}$. Then,

$$f_-(\bar{u}) = \eta|\bar{u} - \bar{d}|^2 + (y + |s|^2 - 2|s|\mathcal{R}e\{\bar{u}\})^2.$$

Separating the real and imaginary parts, we observe

$$f_-(\bar{u}) = \eta(\mathcal{R}e\{\bar{u}\} - \mathcal{R}e\{\bar{d}\})^2 + \eta(\mathcal{I}m\{\bar{u}\} - \mathcal{I}m\{\bar{d}\})^2 + (y + |s|^2 - 2|s|\mathcal{R}e\{\bar{u}\})^2,$$

which is clearly minimized when $\mathcal{I}m\{\bar{u}\} = \mathcal{I}m\{\bar{d}\}$. The real component is quadratic in $\mathcal{R}e\{\bar{u}\}$, so differentiating with respect to $\mathcal{R}e\{\bar{u}\}$ yields

$$\frac{df_+(\bar{u})}{d\mathcal{R}e\{\bar{u}\}} = 2\eta(\mathcal{R}e\{\bar{u}\} - \mathcal{R}e\{\bar{d}\}) + 4|s|(2|s|\mathcal{R}e\{\bar{u}\} - (y + |s|^2)),$$

which is minimized at

$$\mathcal{R}e\{\bar{u}\} = \frac{\eta\mathcal{R}e\{\bar{d}\} + 2|s|(y + |s|^2)}{\eta + 4|s|^2}.$$

This closed form solution yields

$$u_- = (\mathcal{R}e\{\bar{u}\} + i\mathcal{I}m\{\bar{u}\})e^{i\angle s}.$$

Minimizing $f_+(u)$ along the curve $f_+(u) = f_-(u)$ requires parameterizing the curve. Again, define $\bar{u} = ue^{-i\angle s}$, $\bar{d} = de^{-i\angle s}$, and $\bar{s} = |s|$. Note that $\phi_-(\bar{u}; \bar{s}, y) = |\bar{s} - \bar{u}|^2 + (y - |\bar{u}|^2)$, where the latter term equals $B \triangleq -h_+(\bar{u}; y)$. Along the curve $f_+(\bar{u}) = f_-(\bar{u})$, $B^2 = (B + |\bar{s} - \bar{u}|^2)^2$, which is true when $s = \bar{u}$, or when $|\bar{s} - \bar{u}|^2 = -2B = 2(|\bar{u}|^2 - y)$. For this second case to yield a nontrivial solution requires $B < 0$, which corresponds to $|\bar{u}|^2 > y$.

Rearranging terms yields our familiar circle $|\bar{u} + \bar{s}|^2 = 2(y + \bar{s}^2)$ from the Laplace distribution case. Plugging our angular parameterization $\bar{u} = c_0e^{i\theta} - s$, where $c_0 = \sqrt{2(y + \bar{s}^2)}$, into $f_+(\bar{u})$ yields

$$f_+(\bar{u}(\theta)) = (|c_0e^{i\theta} - \bar{s}|^2 - y)^2 + \eta|c_0e^{i\theta} - \bar{s} - \bar{d}|^2 = (c_0^2 - 2c_0\mathcal{R}e\{e^{i\theta}\bar{s}^*\} + \bar{s}^2 - y)^2 + \eta(c_0^2 + |\bar{s} + \bar{d}|^2 - 2c_0\mathcal{R}e\{e^{i\theta}(\bar{s} + \bar{d})^*\}).$$

Let $c_1 = c_0^2 + \bar{s}^2 - y$, and $c_2 = c_0^2 + |\bar{s} + \bar{d}|^2$, so

$$f_+(\bar{u}(\theta)) = (c_1 - 2c_0\mathcal{R}e\{e^{i\theta}\bar{s}^*\})^2 + \eta(c_2 - 2c_0\mathcal{R}e\{e^{i\theta}(\bar{s} + \bar{d})^*\}) = (2c_0)^2\mathcal{R}e\{e^{i\theta}\bar{s}^*\}^2 - 2c_0\mathcal{R}e\{e^{i\theta}(2c_1\bar{s} + \eta(\bar{s} + \bar{d}))^*\} + c_1^2 + \eta c_2.$$

For convenience, let $r_1 = 2c_0\bar{s}$, and r_2 and α be the magnitude and phase of $2c_0(2c_1\bar{s} + \eta(\bar{s} + \bar{d}))$. Differentiating with respect to θ ,

$$\frac{df_+(\bar{u}(\theta))}{d\theta} = r_2 \sin(\theta - \alpha) - 2r_1^2 \sin \theta \cos \theta.$$

Setting the derivative equal to zero,

$$\frac{r_2}{r_1^2} \sin(\theta - \alpha) = \sin(2\theta).$$

Defining ξ such that $\theta = 2\arctan\xi$, we have $\sin\theta = \sin(2\arctan\xi) = \frac{2\xi}{1+\xi^2}$, and $\cos\theta = \cos(2\arctan\xi) = \frac{1-\xi^2}{1+\xi^2}$. Thus,

$$\sin(2\theta) = 2\frac{2\xi(1-\xi^2)}{(1+\xi^2)^2},$$

$$\sin(\theta - \alpha) = \frac{2\xi \cos \alpha - (1-\xi^2) \sin \alpha}{1+\xi^2}.$$

Substituting,

$$0 = \frac{r_2}{r_1^2} (2\xi \cos \alpha - (1-\xi^2) \sin \alpha) (1+\xi^2) - 4\xi(1-\xi^2) = \frac{r_2}{r_1^2} (2\xi \cos \alpha + 2\xi^3 \cos \alpha - \sin \alpha + \xi^4 \sin \alpha) - 4\xi(1-\xi^2) = \left(\frac{r_2}{r_1^2} \sin \alpha\right) \xi^4 + \left(2\frac{r_2}{r_1^2} \cos \alpha + 4\right) \xi^3 + \left(2\frac{r_2}{r_1^2} \cos \alpha - 4\right) \xi - \frac{r_2}{r_1^2} \sin \alpha.$$

This quartic equation can be solved analytically; the real root that corresponds to θ with the minimum $f_+(\bar{u}(\theta))$ is used to generate $u_{\pm} = (c_0e^{i\theta} - \bar{s})e^{i\angle s}$, which is valid as long as $|u_{\pm}|^2 > y$. Also, one must consider $\theta = \pm\pi$, which correspond to $\xi = \pm\infty$, in case either extreme point minimizes $f_+(\bar{u}(\theta))$.

ACKNOWLEDGMENTS

The authors would like to acknowledge Yoav Shechtman for insights relating to phase retrieval and coherent diffraction imaging, and for sharing image data, and James Fienup for general discussions on phase retrieval.

REFERENCES

- [1] J. R. Fienup, "Phase retrieval algorithms: a personal tour [Invited]," *Appl. Optics*, vol. 52, no. 1, pp. 45–56, Jan. 2013.
- [2] Y. Shechtman, Y. C. Eldar, O. Cohen, H. N. Chapman, J. Miao, and M. Segev, "Phase retrieval with application to optical imaging," *IEEE Signal Processing Magazine*, to appear.
- [3] M. V. Klibanov, P. E. Sacks, and A. V. Tikhonravov, "The phase retrieval problem," *Inverse Prob.*, vol. 11, no. 1, pp. 1–28, Feb. 1995.
- [4] D. Sayre, "Some implications of a theorem due to Shannon," *Acta Cryst.*, vol. 5, p. 843, 1952.
- [5] R. P. Millane, "Phase retrieval in crystallography and optics," *J. Opt. Soc. Am. A*, vol. 7, no. 3, pp. 394–411, Mar. 1990.
- [6] H. A. Hauptman, "The phase problem of X-ray crystallography," *Reports on Progress in Physics*, vol. 54, no. 11, pp. 1427–54, Nov. 1991.
- [7] R. W. Harrison, "Phase problem in crystallography," *J. Opt. Soc. Am. A*, vol. 10, no. 5, pp. 1046–55, May 1993.
- [8] A. Walther, "The question of phase retrieval in optics," *Optica Acta: Intl. J. of Optics*, vol. 10, no. 1, pp. 41–9, 1963.
- [9] J. R. Fienup and J. C. Dainty, "Phase retrieval and image reconstruction for astronomy," in *Image Recovery: Theory and Application*, H. Stark, Ed. San Diego: Academic, 1987, pp. 231–275.
- [10] J. Miao, P. Charalambous, J. Kirz, and D. Sayre, "Extending the methodology of X-ray crystallography to allow imaging of micrometre-sized non-crystalline specimens," *Nature*, vol. 400, no. 6742, pp. 342–4, Jul. 1999.
- [11] R. Balan, P. Casazza, and D. Edidin, "On signal reconstruction without phase," *Applied and Computational Harmonic Analysis*, vol. 20, no. 3, pp. 345–356, May 2006.
- [12] K. Setsompop, L. L. Wald, V. Alagappan, B. A. Gagoski, and E. Adalsteinsson, "Magnitude least squares optimization for parallel radio frequency excitation design demonstrated at 7 Tesla with eight channels," *Mag. Res. Med.*, vol. 59, no. 4, pp. 908–15, Apr. 2008.
- [13] A. Chai, M. Moscoso, and G. Papanicolaou, "Array imaging using intensity-only measurements," *Inverse Prob.*, vol. 27, no. 1, p. 015005, Jan. 2011.
- [14] T. Lатышевская, J.-N. Longchamp, and H.-W. Fink, "Novel Fourier-domain constraint for fast phase retrieval in coherent diffraction imaging," *Optics Express*, vol. 19, no. 20, pp. 19330–9, Sep. 2011.
- [15] A. V. Oppenheim and J. S. Lim, "The importance of phase in signals," *Proc. IEEE*, vol. 69, no. 5, pp. 529–41, May 1981.
- [16] R. W. Gerchberg and W. O. Saxton, "A practical algorithm for the determination of phase from image and diffraction plane pictures," *Optik*, vol. 35, pp. 237–46, Apr. 1972.
- [17] J. R. Fienup, "Reconstruction of an object from the modulus of its Fourier transform," *Optics Letters*, vol. 3, no. 1, pp. 27–9, Jul. 1978.

- [18] —, “Phase retrieval algorithms: a comparison,” *Appl. Optics*, vol. 21, no. 15, pp. 2758–69, Aug. 1982.
- [19] M. H. Hayes and T. F. Quatieri, “Recursive phase retrieval using boundary conditions,” *J. Opt. Soc. Am.*, vol. 73, no. 11, pp. 1427–1433, Nov. 1983.
- [20] J. R. Fienup, “Phase retrieval using boundary conditions,” *J. Opt. Soc. Am. A*, vol. 3, no. 2, pp. 284–288, Feb. 1986.
- [21] —, “Reconstruction of a complex valued object from the modulus of its Fourier transform using a support constraint,” *J. Opt. Soc. Am. A*, vol. 4, no. 1, pp. 118–23, Jan. 1987.
- [22] H. H. Bauschke, P. L. Combettes, and D. R. Luke, “Hybrid projection-reflection method for phase retrieval,” *J. Opt. Soc. Am. A*, vol. 20, no. 6, pp. 1025–34, Jun. 2003.
- [23] H. Ohlsson and Y. C. Eldar, “On conditions for uniqueness in sparse phase retrieval,” in *Proc. IEEE Conf. Acoust. Speech Sig. Proc.*, 2014, pp. 1841–5.
- [24] J. Ranieri, A. Chebira, Y. M. Lu, and M. Vetterli, “Phase retrieval for sparse signals: Uniqueness conditions,” 2013, arxiv 1308.3058. [Online]. Available: <http://arxiv.org/abs/1308.3058>
- [25] Y. C. Eldar and S. Mendelson, “Phase retrieval: Stability and recovery guarantees,” *Applied and Computational Harmonic Analysis*, vol. 36, no. 3, pp. 473–94, May 2014.
- [26] M. L. Moravec, J. K. Romberg, and R. G. Baraniuk, “Compressive phase retrieval,” in *Proc. SPIE 6701 Wavelets XII*, 2007, p. 670120.
- [27] P. Schniter and S. Rangan, “Compressive phase retrieval via generalized approximate message passing,” in *Proc. 50th Allerton Conf. on Comm., Control, and Computing*, 2012, pp. 815–822.
- [28] S. Mukherjee and C. S. Seelamantula, “An iterative algorithm for phase retrieval with sparsity constraints: application to frequency domain optical coherence tomography,” in *Proc. IEEE Conf. Acoust. Speech Sig. Proc.*, 2012, pp. 553–6.
- [29] E. Osherovich, M. Zibulevsky, and I. Yavneh, “Approximate fourier phase information in the phase retrieval problem: what it gives and how to use it,” *J. Opt. Soc. Am. A*, vol. 28, no. 10, pp. 2124–2131, Oct. 2011.
- [30] E. J. Candès, T. Strohmer, and V. Voroninski, “PhaseLift: exact and stable signal recovery from magnitude measurements via convex programming,” *Comm. Pure Appl. Math.*, vol. 66, no. 8, pp. 1241–74, Aug. 2013.
- [31] E. J. Candès, Y. C. Eldar, T. Strohmer, and V. Voroninski, “Phase retrieval via matrix completion,” *SIAM J. Imaging Sci.*, vol. 6, no. 1, pp. 199–225, 2013.
- [32] L. Demanet and V. Jugnon, “Convex recovery from interferometric measurements,” 2013, arxiv 1307.6864. [Online]. Available: <http://arxiv.org/abs/1307.6864>
- [33] Y. Shechtman, Y. C. Eldar, A. Szameit, and M. Segev, “Sparsity based sub-wavelength imaging with partially incoherent light via quadratic compressed sensing,” *Optics Express*, vol. 19, no. 16, pp. 14807–22, Aug. 2011.
- [34] H. Ohlsson, A. Y. Yang, R. Dong, and S. S. Sastry, “Compressive phase retrieval from squared output measurements via semidefinite programming,” 2012, arxiv 1111.6323. [Online]. Available: <http://arxiv.org/abs/1111.6323>
- [35] X. Li and V. Voroninski, “Sparse signal recovery from quadratic measurements via convex programming,” *SIAM J. Math. Anal.*, vol. 45, no. 5, pp. 3019–33, 2013.
- [36] I. Waldspurger, A. d’Aspremont, and S. Mallat, “Phase recovery, maxcut and complex semidefinite programming,” *Mathematical Programming*, pp. 1–35, Dec. 2013.
- [37] K. Jaganathan, S. Oymak, and B. Hassibi, “Recovery of sparse 1-d signals from the magnitudes of their Fourier transform,” in *Intl. Symp. on Information Theory*, 2012, pp. 1473–7.
- [38] Y. Shechtman, A. Beck, and Y. C. Eldar, “GESPAR: efficient phase retrieval of sparse signals,” *IEEE Trans. Sig. Proc.*, vol. 62, no. 4, pp. 928–38, Feb. 2014.
- [39] D. S. Weller, A. Pnueli, O. Radzyner, G. Divon, Y. C. Eldar, and J. A. Fessler, “Phase retrieval of sparse signals using optimization transfer and ADMM,” in *Proc. IEEE Intl. Conf. on Image Processing*, 2014, pp. 1342–6.
- [40] S. Boyd and L. Vandenberghe, *Convex optimization*. UK: Cambridge, 2004.
- [41] K. Lange, D. R. Hunter, and I. Yang, “Optimization transfer using surrogate objective functions,” *J. Computational and Graphical Stat.*, vol. 9, no. 1, pp. 1–20, Mar. 2000.
- [42] M. W. Jacobson and J. A. Fessler, “An expanded theoretical treatment of iteration-dependent majorize-minimize algorithms,” *IEEE Trans. Im. Proc.*, vol. 16, no. 10, pp. 2411–22, Oct. 2007.
- [43] R. Glowinski and A. Marrocco, “Sur l’approximation par éléments nis dordre un, et la resolution par penalisation-dualite dune classe de problemes de dirichlet nonlineaires, rev. francaise daut,” *Inf. Rech. Oper.*, vol. R-2, pp. 41–76, 1975.
- [44] D. Gabay and B. Mercier, “A dual algorithm for the solution of nonlinear variational problems via finite-element approximations,” *Comput. Math. Appl.*, vol. 2, no. 1, pp. 17–40, 1976.
- [45] J. Eckstein and D. P. Bertsekas, “On the Douglas-Rachford splitting method and the proximal point algorithm for maximal monotone operators,” *Mathematical Programming*, vol. 55, no. 1-3, pp. 293–318, Apr. 1992.
- [46] S. Boyd, N. Parikh, E. Chu, B. Peleato, and J. Eckstein, “Distributed optimization and statistical learning via the alternating direction method of multipliers,” *Found. & Trends in Machine Learning*, vol. 3, no. 1, pp. 1–122, 2010.
- [47] S. S. Chen, D. L. Donoho, and M. A. Saunders, “Atomic decomposition by basis pursuit,” *SIAM J. Sci. Comp.*, vol. 20, no. 1, pp. 33–61, 1998.
- [48] D. L. Donoho and M. Elad, “Optimally sparse representation in general (nonorthogonal) dictionaries via l_1 minimization,” *Proc. Natl. Acad. Sci.*, vol. 100, no. 5, pp. 2197–2202, Mar. 2003.
- [49] J. A. Tropp, “Greed is good: algorithmic results for sparse approximation,” *IEEE Trans. Info. Theory*, vol. 50, no. 10, pp. 2231–42, Oct. 2004.
- [50] A. Beck and M. Teboulle, “A fast iterative shrinkage-thresholding algorithm for linear inverse problems,” *SIAM J. Imaging Sci.*, vol. 2, no. 1, pp. 183–202, 2009.
- [51] T. Goldstein and S. Osher, “The split Bregman method for L_1 -regularized problems,” *SIAM J. Imaging Sci.*, vol. 2, no. 2, pp. 323–43, 2009.
- [52] A. Beck and M. Teboulle, “Fast gradient-based algorithms for constrained total variation image denoising and deblurring problems,” *IEEE Trans. Im. Proc.*, vol. 18, no. 11, pp. 2419–34, Nov. 2009.
- [53] Y. Wang, J. Yang, W. Yin, and Y. Zhang, “A new alternating minimization algorithm for total variation image reconstruction,” *SIAM J. Imaging Sci.*, vol. 1, no. 3, pp. 248–72, 2008.
- [54] Z. Tan, Y. C. Eldar, A. Beck, and A. Nehorai, “Smoothing and decomposition for analysis sparse recovery,” *IEEE Trans. Sig. Proc.*, vol. 62, no. 7, pp. 1762–74, Apr. 2014.
- [55] N. Parikh and S. Boyd, “Proximal algorithms,” *Found. Trends in Optimization*, vol. 1, no. 3, pp. 123–231, 2013.
- [56] R. Fletcher and C. M. Reeves, “Function minimization by conjugate gradients,” *Comput. J.*, vol. 7, no. 2, pp. 149–54, 1964.
- [57] A. Szameit, Y. Shechtman, E. Osherovich, E. Bullkich, P. Sidorenko, H. Dana, S. Steiner, E. B. Kley, S. Gazit, T. Cohen-Hyams, S. Shoham, M. Zibulevsky, I. Yavneh, Y. C. Eldar, O. Cohen, and M. Segev, “Sparsity-based single-shot subwavelength coherent diffractive imaging,” *Nature Materials*, vol. 11, p. 4559, Apr. 2012.
- [58] D. S. Weller, S. Ramani, J.-F. Nielsen, and J. A. Fessler, “Monte Carlo SURE-based parameter selection for parallel magnetic resonance imaging reconstruction,” *Mag. Res. Med.*, vol. 71, no. 5, pp. 1760–70, May 2014.
- [59] E. J. Candès, X. Li, and M. Soltanolkotabi, “Phase retrieval via Wirtinger flow: Theory and algorithms,” 2014, arxiv 1407.1065. [Online]. Available: <http://arxiv.org/abs/1407.1065>
- [60] Y. Nesterov, “A method of solving a convex programming problem with convergence rate $O(1/k^2)$,” *Soviet Math. Dokl.*, vol. 27, no. 2, pp. 372–76, 1983.